Numerical calculation of 3D eddy current fields in transverse flux machines with time stepping procedures

Rolf Blissenbach and Gerhard Henneberger
Department of Electrical Machines,
Aachen Institute of Technology (RWTH), Germany

Keywords *Transverse flux, Eddy current, Finite elements*

Abstract *Presents the calculation of the induced eddy currents in the conducting parts of transverse flux machines. Compared to conventional machines the transverse flux machine has a bigger torque, both with respect to volume and weight. For this reason, it is especially suited for direct drive applications in electric vehicles and railways. The main focus in this paper is the investigation of the different loss mechanisms caused by the sinusoidal stator current and the movement of the permanent magnet excited rotor. A 3D FEM solver with a* $\vec{A} - \vec{A}, \vec{T}$ *potential formulation is used in combination with edge elements. The time stepping procedure, with special focus on the displacement between stator and rotor mesh for the velocity effect, is explained in detail. The eddy current density distribution in the different parts of the machine is shown.*

Introduction

Different topologies of transverse flux machines have been developed at the Department of Electrical Machines in Aachen (Bork and Henneberger, 1996; Blissenbach and Henneberger, 1999 a,b). In the lower power range, transverse flux motors have an excellent torque-to-volume ratio in comparison with conventional machines. The reason for the high specific torque is the decoupling of magnetic flux paths and armature coils, which allows a very high current loading and consequently a high force density by simply enlarging the number of pole pairs. For this reason, it is especially suited for direct drive applications in electric vehicles and railways. All developed topologies are permanent magnet excited three phase designs with an external rotor and a water-cooled stator with ring windings. Carriers with suitable geometry and material have to be chosen for both stator and rotor in order to mount the active parts. In case of conducting carrier regions the investigation of eddy current losses in these parts is very important for the prediction of the machine performance. To prevent the risk of demagnetization of the NdFeB magnets, which have a good electric conductivity, at high temperature, the eddy currents in the magnets also have to be examined.

The different loss mechanisms have been calculated with a simplified technique in Bork *et al.* (1998), which nevertheless has led to quite good results.

COMPEL : The International Journal for Computation and Mathematics in Electrical and Electronic Engineering, Vol. 20 No. 1, 2001, pp. 152-166.

The spatial change of the magnetic conductivity in the stator and armature reaction in case of rotating rotor cause eddy currents both in the magnetically active and passive parts in the rotor. But especially for these rotor losses only a rough estimation could be done with the applied technique. Therefore, in this paper a 3D FEM solver with time stepping procedure is used, which is also capable of simulating the rotor movement.

Design of the machine

Magnetic circuit

The geometry of the magnetic circuit is presented in Figure 1. For a better view the figure only shows one pole of one phase in a linear arrangement.

The complete machine consists of three phases. The armature winding in the inner stator is surrounded by U-shaped soft iron parts, which are arranged circumferentially in a distance of a double pole pitch. The limbs of the U-yoke are shifted by an electrical angle of 180° against each other. The U-yoke lamination is stacked in circumferential direction. The geometrical shift is achieved by bending the complete stack before bonding.

In order to get the utilization of the magnetic circuit as high as possible, the cross sections of the U-cores get bigger at the air gap by using pole shoes. The small overhanging pieces at the outer edges of the pole shoes are used for the fixation of the U-cores with a banding around the complete periphery. In the external rotor a flux concentrating design with soft magnetic pieces between the rare earth permanent magnets, which are magnetized with alternating polarity in circumferential direction, is applied. The magnetic flux is of three dimensional nature in the flux concentrating parts in the rotor. Therefore they have to be made of a soft magnetic composite (powder iron) material instead of laminated iron.

The magnetic properties of the soft magnetic composite material are worse than the properties of a good laminated steel and even the hysteresis losses at

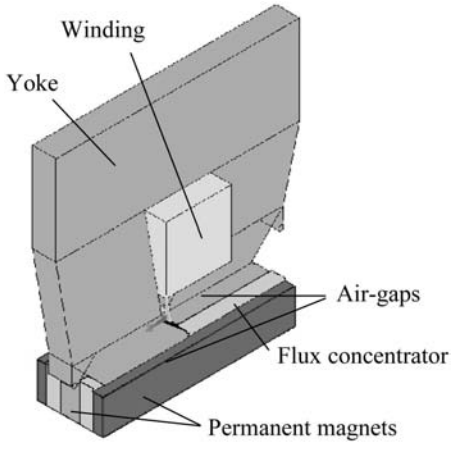

Figure 1.
Linearized pole of the magnetic circuit

low frequencies are much higher, but the guidance of the flux in three dimensions is impossible with laminated steel. The reason is the occurrence of high eddy current losses caused by alternating fields perpendicular to the direction of lamination.

Mechanical arrangement

The complete three phase design is shown in Figure 2. In contrast to conventional machines, there is no common rotating field in the three phase design of a transverse flux machine, but only three independent alternating fields which are electrically shifted by 120°.

The necessary mechanical shift is done in the rotor by shifting the complete rotor rings, consisting of the magnets and the powder iron parts, from one phase to the next. Accordingly, the stator cores in all phases can be arranged in line. In contrast to the design described in Bork (1996) the three phases need no axial space between each other. This reduces the axial length and results in a partial magnetic coupling between the phases. Therefore the flux sharing central yokes only need an axial length of $\sqrt{3} \cdot a$ with a being the axial length of the outer yokes.

Because of the magnetic coupling and the displacement between the limbs of the U-cores, the rotor rings only need an electrical shift of 60° from one phase to the next. The risk of a stray flux between two adjacent rings is therefore reduced. With the use of a standard inverter the currents in the three windings are shifted electrically 120°.

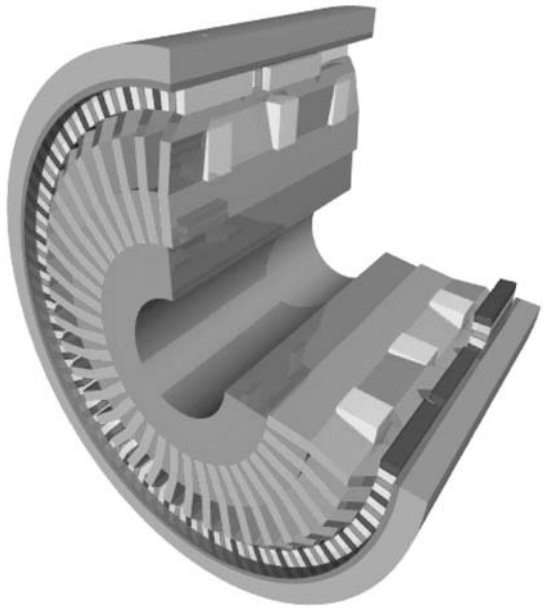

Figure 2.
Design of the three phase transverse flux machine

The selection of the carrier materials is difficult for the stator and the rotor, because stray field components are expected in these passive parts. Therefore the fixation of the active rotor parts and the U-yokes has to be non-magnetic and in the optimal case electrically insulating to avoid eddy currents caused by stray fluxes, but heat-conducting for the heat discharge of the rotor losses. Naturally a compromise has to be found here.

As it has been mentioned before, the stator yokes are made of laminated steel, which makes the direct calculation of eddy currents in this region quite difficult. The reason is the very big number of finite elements in a model, which allows for the lamination. Therefore, the calculation of eddy current losses is done at first only in the rotor region. Another reason for this approach is the cooling of the machine. The heat discharge in the stator yokes is quite good because of the water cooling in the inner stator. The cooling of the external rotor is more difficult and especially the permanent magnets show critical behavior with rising temperature. Hence, the investigation of the loss mechanisms in the rotor is very important.

The different active and passive parts in the rotor are shown in Figure 3. The permanent magnets are inserted between the flux concentrating pieces, made of a soft magnetic composite material. This material tends to have very low eddy currents because the conduction between grains is very small. The flux concentrating pieces are therefore not defined as an eddy current region in the numerical calculation. In contrast to the powder iron, the NdFeB permanent magnets have a quite good electric conductivity.

The complete arrangement of the active parts is framed by a ring made of a non-magnetic material to prevent high stray fluxes from one soft magnetic piece to the other. The electric conductivity of this material is very high for using the ring as a damper to displace magnetic flux from the carrier adjacent to the ring. The carrier itself is also made of a non-magnetic

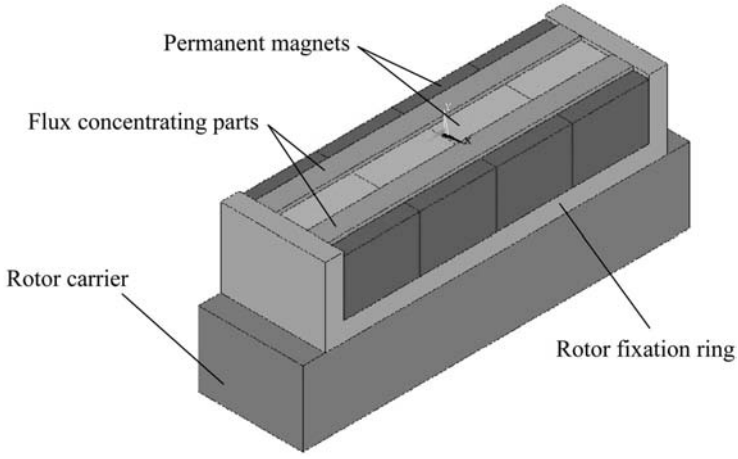

Figure 3.
Active and passive rotor regions in the transverse flux machine

material with a good electric conductivity. All the material properties are given in Table I.

Eddy current calculation methods

Vector potential formulation $\overrightarrow{A} - \overrightarrow{A}, \overrightarrow{T}$

The potential formulation is using the magnetic vector potential $\overrightarrow{A}$ in the regions without eddy currents and both the magnetic and electric vector potential $\overrightarrow{T}$ in the eddy current regions. This leads to the same potential derivations for the magnetic and electric field together in one region (Albertz, 1999):

$$\vec{B} = curl\ \vec{A}\ \ ;\ \ \vec{J} = curl\ \vec{T}\ . \tag{1}$$

The Galerkin potential equation in the regions without eddy currents results to:

$$\int_{\Omega} curl\ \vec{\alpha}_i \cdot \upsilon\ curl\ \vec{A}(t)d\Omega = \int_{\Omega} (\vec{\alpha}_i \cdot \vec{J}(t) + curl\ \vec{\alpha}_i \cdot \upsilon \vec{B}_r)d\Omega \tag{2}$$

and in the regions with eddy currents:

$$\begin{aligned} &\int_{\Omega} (curl\ \vec{\alpha}_i \cdot \upsilon\ rot\ \vec{A}(t) - \vec{\alpha}_i \cdot curl\ \vec{T}(t))d\Omega = 0 \\ &\wedge \int_{\Omega} (curl\ \vec{\alpha}_i \cdot \frac{1}{\sigma} rot\ \vec{T}(t) + curl\ \vec{\alpha}_i \cdot \frac{\partial}{\partial t}\vec{A}(t))d\Omega = 0 \end{aligned} \tag{3}$$

The time discretization of a general vector $\overrightarrow{u}(t)$ is done with a linear time interpolation between two time steps t_n and t_{n+1}:

$$\vec{u}(t) = \vec{u}_{n+1} \cdot \frac{t - t_n}{t_{n+1} - t_n} + \vec{u}_n \cdot \frac{t_{n+1} - t}{t_{n+1} - t_n} \quad \text{for} \quad t_n \le t \le t_{n+1} \tag{4}$$

With the use of a time dependent function

	Magnetic property (relative permeability)	Electric property (resistivity)
Rotor carrier	$\mu_r = 1$	$\rho = 20\mu\Omega$ cm
Rotor ring	$\mu_r = 1$	$\rho = 5\mu\Omega$ cm
Permanent magnet	$\mu_r = 1.07$	$\rho = 130\mu\Omega$ cm
Soft magnetic composite	Nonlinear	$\rho =$ infinite

Table I.
Material properties of the rotor regions

$$\tau(t) = \frac{t - t_n}{t_{n+1} - t_n} \quad \text{for} \quad t_n \leq t \leq t_{n+1} \tag{5}$$

the vector $\overrightarrow{u}(t)$ results to:

$$\vec{u}(t) = \vec{u}_{n+1} \cdot \tau(t) + \vec{u}_n \cdot (1 - \tau(t)) \quad \text{for} \quad 0 \leq \tau(t) \leq 1 \tag{6}$$

For all vector functions in the potential equation this approach is applied. The choice of the value for τ shows big influence on the solution. All the following calculations were done with $\tau = {}^2/_3$ (Galerkin).

FEM model and mesh

The FEM model of the transverse flux machine only consists of a section of one phase including a double pole pitch in circumferential direction, which is the smallest symmetry unit of the machine. Comparative investigations between linear and rotationally symmetric FE-models have shown that the consideration of a geometrically linear model is sufficient, because of the small pole pitch. The mesh for the non-air parts of the FE-model is shown in Figure 4. The total mesh including the air regions consists of 250,000 tetrahedral elements and 50,000 nodes.

The mesh for the eddy current regions in the rotor, which consist of the permanent magnets and the carrier parts, has to be influenced by the penetration depth δ of the electromagnetic field:

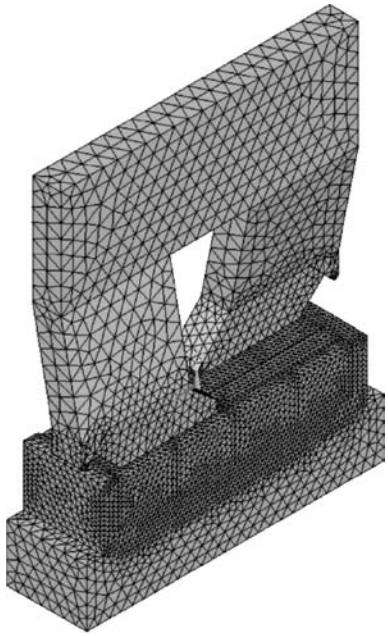

Figure 4.
FEM mesh of the transverse flux machine

$$\delta = \frac{1}{\sqrt{\pi \cdot f \cdot \sigma \cdot \mu}} \quad . \tag{7}$$

Special attention has to be paid to the periodic boundary conditions of the FE-model in circumferential direction. The mesh in both edge layers has to be exactly the same to apply a periodic boundary condition. Therefore, one of the edge layers is meshed with triangle elements and then copied on the other edge layer. After this operation the three-dimensional meshing of the model with tetrahedral elements is done. The chosen approach for the mesh generation is therefore a combination of two- and three-dimensional meshing.

Rotor movement

Another important point for the meshing of the model is the simulation of the rotor movement. The applied technique permits the use of only one mesh for the complete transient calculation.

This is realized with a layer in the airgap between stator and rotor, which has exactly the same mesh in equidistant spacing Δx in the direction of movement. This equidistant spacing is depending on the desired geometric step width from one time step to the next. The simplest strategy of producing this meshed layer is to mesh only a part of the layer with the width Δx and then copy this mesh in the direction of movement. After every rotor position change of $n \cdot \Delta x$ the positions of the nodes in the layer are congruent again. Therefore, stator and rotor mesh are completely independent and they are shifted against each other, but it is not necessary to mesh the airgap region again. Only the constraints have to be defined new after each transient step. The rotor displacement of one pole pitch is shown in Figure 5. Depending on the rotor position the sinusoidal stator current is fed into the winding.

Results

Blocked rotor

The first calculations were done for a blocked rotor, which means that there is no velocity in the model, and a sinusoidal current in the stator winding. This operating point has been investigated first because of its faster convergence. The stator current has a value of 250A and a frequency of 50Hz. The rotor stands in the position of maximum excitation flux. But the more interesting investigation is of course the operation with moved rotor. Therefore, the results for the blocked rotor shown here only give an overview of the loss mechanisms.

The current density distribution in the eddy current regions in the rotor is shown in Figure 6. The highest eddy current losses are in the damper ring, which has been inserted in the rotor to displace magnetic flux from the carrier. The losses in the magnets are quite low and should not lead to a critical heating

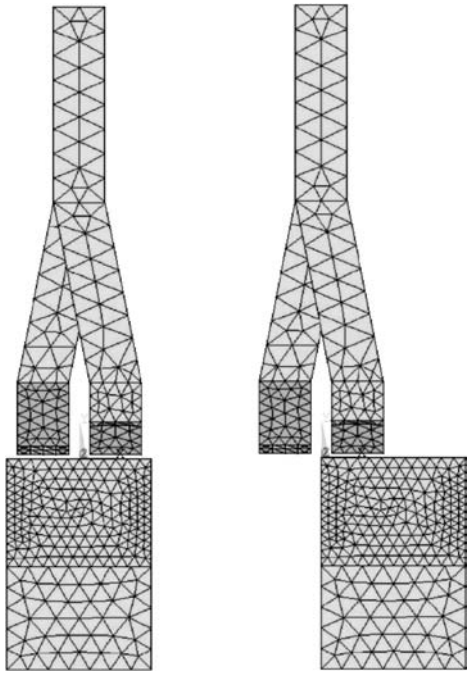

Figure 5.
Displacement of the rotor and stator mesh

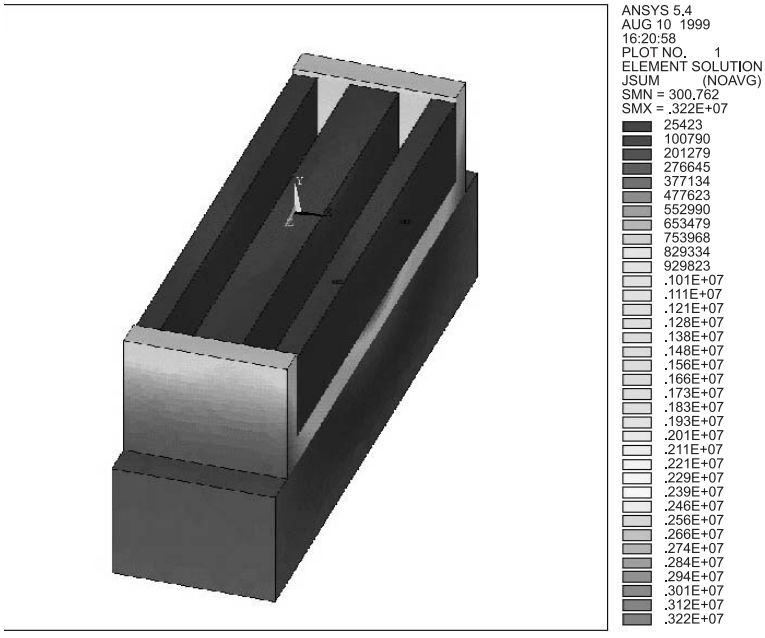

Figure 6.
Eddy current distribution in the blocked rotor

of the magnets. But the heat discharge of the adjacent rings into the permanent magnets could cause problems with overheating in these parts. The losses in the different rotor regions are given in Table II in relation to the total eddy current losses.

Moved rotor

As it has been explained above, the FEM model is also prepared for the calculation of the moved rotor. Reaching the convergence is here more difficult and therefore at first the calculations are done for low frequencies and velocities. For the investigation of the loss mechanisms in the different regions this should be sufficient. The operating point is the same as in the case with blocked rotor. The current density distribution in the eddy current regions in the rotor is shown in Figures 7, 8 and 9. The figures all show the rotor position with the highest eddy current losses. In order to get a better overview of the losses, the different regions are shown separately. For the comparison of the current density, the different scaling in the figures has to be taken into account.

The highest eddy current losses are again in the damper ring. The idea of displacing the magnetic flux from the carrier with the damper ring has therefore big disadvantages concerning the total losses. As a result of the calculations the fixation rings for the active parts in the rotor have to be made of a non-magnetic but also non-conductive material. The eddy current losses in the carrier region are quite small for this frequency, but calculations for higher frequencies have to be done to estimate possible heating problems. The small penetration of the magnetic field into the carrier allows eventually the application of a magnetic material for this part of the machine. An important demand for a direct drive application is the mechanical strength of the carrier parts and this can be fulfilled better with a steel alloy, which normally has good magnetic properties. This point will be investigated in the following chapter.

The losses in the magnets are again quite low and should not lead to a critical heating of the magnets. But the heat discharge of the adjacent rings into the permanent magnets is again problematic.

The losses in the different rotor regions are given in Table III in relation to the total eddy current losses. In comparison to the calculation with blocked rotor the total losses are about 50 percent higher.

Table II.
Eddy current losses in the blocked rotor

	Eddy current losses (percentage) operating point: 250A, 50Hz %
Rotor carrier	14.7
Rotor rings	83.9
Permanent magnets	1.4

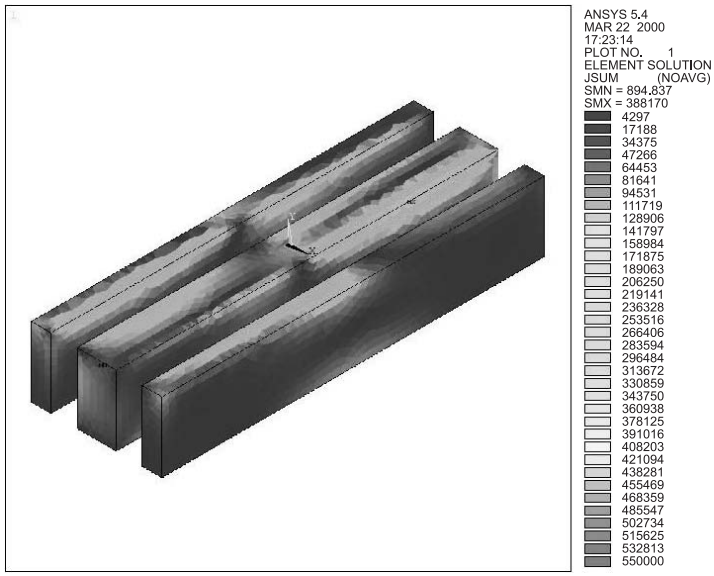

Figure 7.
Eddy current distribution in the permanent magnets with moved rotor

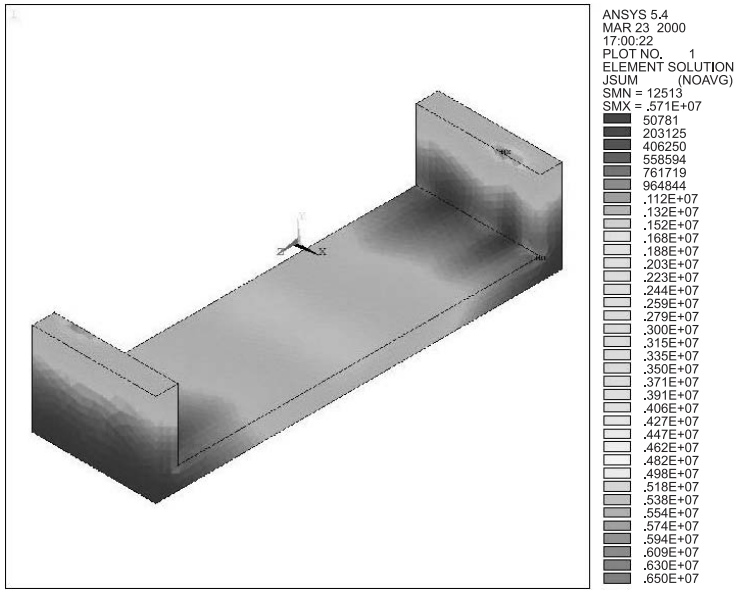

Figure 8.
Eddy current distribution in the rotor ring with moved rotor

Concerning the total computing time, several points have to be taken into account. Two of them are the convergence within one transient step and the number of transient steps for reaching the steady-state condition. The convergence within one transient step is shown in Figure 10 for solutions with different definition of eddy current regions.

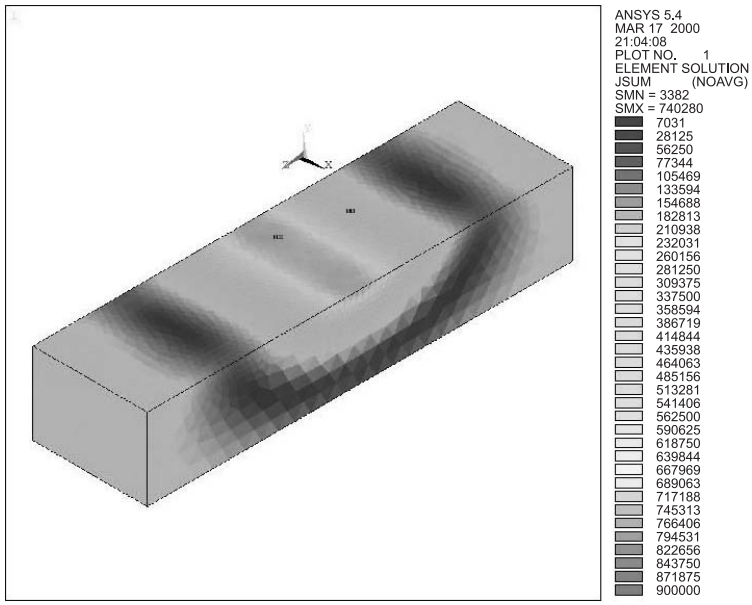

Figure 9.
Eddy current distribution in the rotor carrier with moved rotor

	Eddy current losses (percentage) working point: 250A, 50Hz %
Rotor carrier	12.0
Rotor rings	86.1
Permanent magnets	1.9

Table III.
Eddy current losses in the moved rotor

The upper left figure shows the results obtained with a static solver, the upper right figure describes the transient calculation without the definition of eddy current regions. This calculation needs one more Newton-Raphson step to reach convergence. The number of conjugate gradient steps is for both cases quite low.

The lower left figure shows the results for only one eddy current region in the permanent magnets. The behavior is quite similar to those without eddy current regions. The lower right figure gives the results for the definition of the complete rotor as an eddy current region. The oscillations from one CG-step to the next are high and the number of CG-steps is increased drastically. The main reason for this behavior is not the increased number of eddy current regions but the much lower resistivity of the additional eddy current regions. This leads to the oscillations between the CG-steps and the bad convergence.

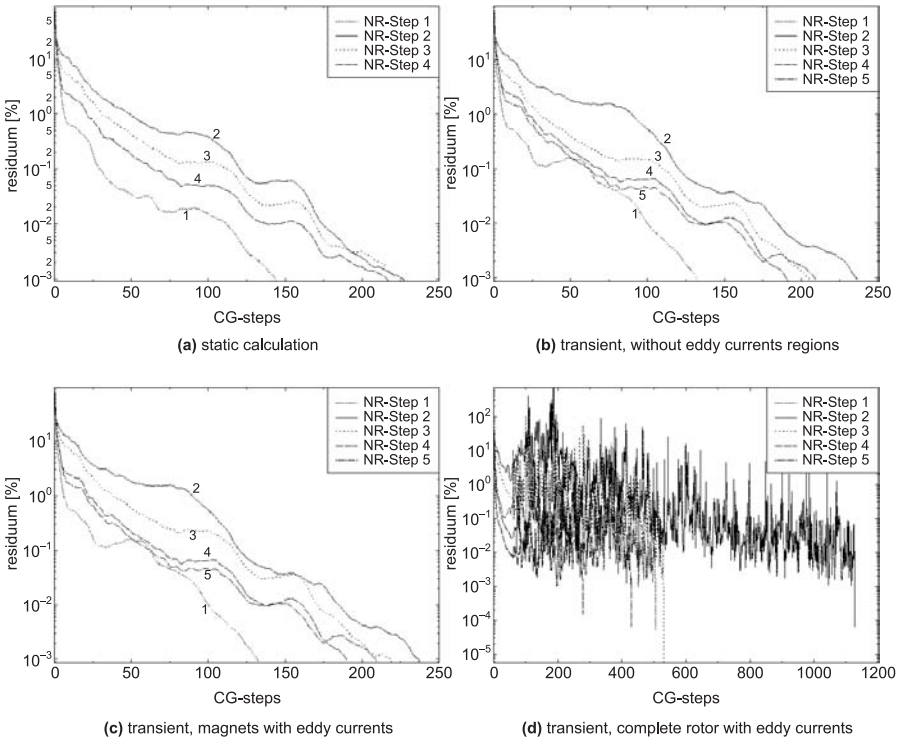

Figure 10.
Convergence with different definition of eddy current regions

The number of transient steps for reaching the steady-state condition is shown in Figure 11 for the different rotor regions. The logarithmic scaling for the losses has to be taken into account.

The rotor movement of a double pole pitch appropriate to a complete period of the sinusoidal stator current is divided into 20 transient steps. After an initial response a periodic behavior concerning the losses can be found with respectively ten transient steps. The same behavior can be found for the calculated forces. A steady state solution is reached after only a few periods because the transverse flux machine is not a rotating field but only an alternating field machine with a simple operation principle.

Magnetic carrier

As it has been mentioned above, the small penetration of the magnetic field into the carrier allows eventually the application of a magnetic material for this part of the machine. The needed mechanical strength of the carrier parts can be fulfilled better with a steel alloy, which normally has good magnetic properties. Therefore, a steel alloy material with a nonlinear B(H)-curve is applied for the carrier. The resistivity is about $\rho = 50\mu\Omega$cm and consequently higher than the value of the non-magnetic material.

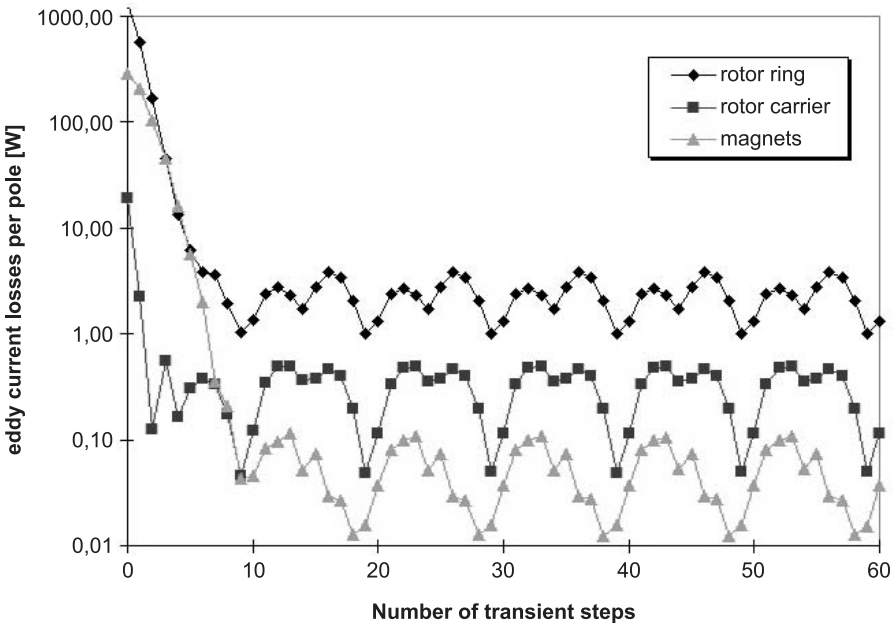

Figure 11.
Number of transient steps for steady state condition

The comparison of the current density in the magnetic (upper) and non-magnetic carrier (lower) is shown in Figure 12. The much higher eddy currents and consequently losses, in the magnetic carrier are obvious. The reason is the occurrence of very big stray fluxes in the magnetic carrier. The losses in the carrier are increased by the factor ten. The losses in the other rotor regions remain nearly unchanged.

Thus, it is definitely impossible to build the carrier with a steel alloy with good magnetic properties, although the mechanical strength would be bigger.

Conclusions

For the first time, the calculation of the induced eddy current fields in the conducting rotor parts of a transverse flux machine is introduced. The calculation is based on a 3D finite element method with a time-stepping procedure. The potential formulation is using two vector potentials for the magnetic and electric field.

With this approach the investigation of the influence of the sinusoidal stator current and particularly the movement of the permanent magnet excited rotor on the eddy current losses is possible. The extracted perceptions of the different loss mechanisms are used for the choice of suitable materials for especially the passive rotor parts, e.g. carriers and fixations.

The convergence of the transient calculation is strongly influenced by the resistivity of the eddy current regions with the presented approach. A steady state solution is reached after only a few periods because the transverse flux

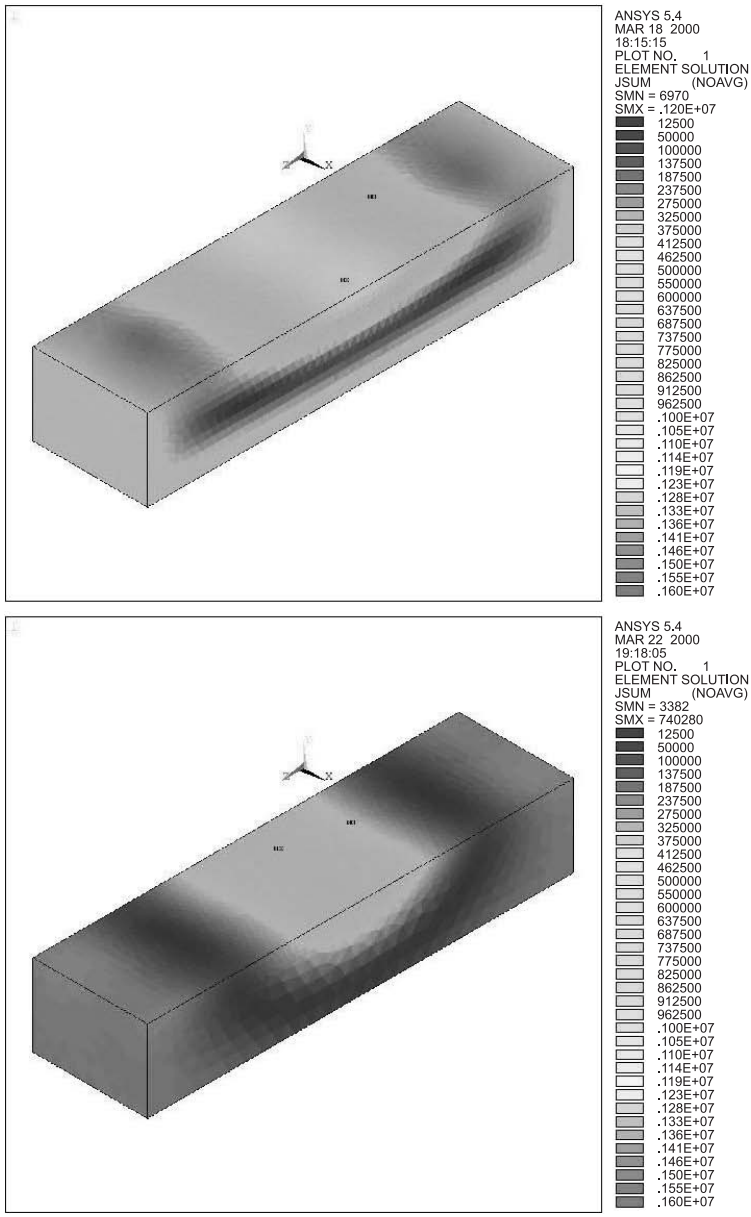

Figure 12.
Comparison of current density in the magnetic (upper) and non-magnetic (lower) carrier

machine is not a rotating field but only an alternating field machine with a simple operation principle.

References

Albertz, D. (1999), "Calculation of 3D eddy current fields using both electric and magnetic vector potential in conducting regions", *IEEE Trans. Magn.*, Vol. 34, No. 5, pp. 2644-7.

Blissenbach, R. and Henneberger, G. (1999a), "Transverse flux motor with high specific torque and efficiency for a direct drive of an electric vehicle", *Proc. ISATA, Clean Power Sources and Environmental Implications in the Automotive Industry*, pp. 429-36.

Blissenbach, R. and Henneberger, G. (1999b), "New design of a transverse flux machine for a wheel hub motor in a tram", *Proc. PCIM, Intelligent Motion*, pp. 189-94.

Bork, M. and Henneberger, G. (1996), "New transverse flux concept for an electric vehicle drive system", *Proc. Int. Conference on Electrical Machines (ICEM)*, Vol. 2, pp. 308-13.

Bork, M., Blissenbach, R. and Henneberger, G. (1998), "Identification of the loss distribution in a transverse flux machine", *Proc. Int. Conference on Electrical Machines (ICEM)*, Vol. 3, pp. 1826-31.